Bioconjugate Chemistry

pubs.acs.org/bc

Article

Noncovalent Fluorescent Biodot–Protein Conjugates with Well-Preserved Native Functions for Improved Sweat Glucose Detection

Xin Ting Zheng,* Yoonah Choi, Darren Guan Ge Phua, and Yen Nee Tan*

Cite This: https://dx.doi.org/10.1021/acs.bioconjchem.9b00856

Read Online

ACCESS | Metrics & More | Article Recommendations | Supporting Information

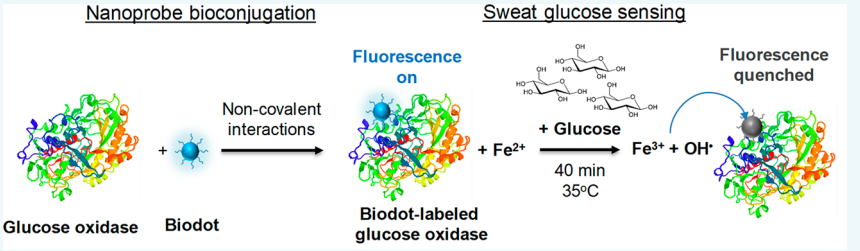

ABSTRACT: To overcome the traditional issues of protein labeling, we report herein an effective approach for noncovalent conjugation of the biomolecule-derived fluorescent nanodots (biodot) to functional proteins without the addition of chemical linkers for biosensor development. The as-prepared fluorescent biodot–protein conjugates are very stable near physiological pH, exhibiting excellent photostability and thermal stability. More importantly, the native functions of proteins, including drug binding and enzymatic activities, are well-preserved after conjugating with biodots. The optimized protein conjugation strategy is then applied to prepare biodot-glucose oxidase (GOx) fluorescent sensing probes for sweat glucose detection. Results show that the as-prepared sensing probes could achieve better assay performance than those covalent conjugates as demonstrated herein. Specifically, GOx in the noncovalently bound conjugates are able to catalyze the oxidation of glucose effectively, which generates hydrogen peroxide as a byproduct. In the presence of Fe^{2+}, Fenton reaction takes place to produce hydroxyl radicals and Fe^{3+}, leading to significant fluorescence quenching of biodots on the conjugates. This simple one-step enzymatic assay in a single probe achieves a wide linear range of 25–1000 μM (R^2 = 0.99) with a low detection limit of 25 μM. Furthermore, negligible interference is observed in the complex artificial sweat sample for accurate glucose quantification, achieving an excellent recovery rate of 100.5 ± 2.2%. This work provides a facile conjugation method that is generally applicable to a wide range of proteins, which will help to accelerate future development of multifunctional fluorescent probes to provide optical signals with unique protein functions (e.g., enzymatic, recognition, etc.) for biomedical sensing and imaging.

INTRODUCTION

Bioconjugation, a process where a biomolecule is linked with a signal molecule, very often a fluorophore, is the most critical step toward successful biosensor development. The popular conjugation methods include genetically encoding with fluorescent proteins[1] and chemically cross-linking with organic fluorophores,[2−4] aggregation-induced emission (AIE) molecules,[5] metal nanoclusters,[6−8] semiconductor quantum dots,[9−11] or carbon dots.[12−17] These bioconjugation methods can be categorized as covalent or noncovalent conjugation. Unlike covalent conjugation where a stable bond is formed, noncovalent conjugation involves cooperative effects of several interactions, which include affinity interaction, electrostatic interaction, metal-mediated coordination, hydrophobic interaction, and hydrogen bonding.[18,19] Although noncovalent interactions are usually weaker than the covalent bonds, noncovalent conjugation still offers critical advantages over covalent bioconjugation as it eliminates tedious procedures, toxic reagents, and the high possibility of protein inactivation due to the random blocking of active sites.[18]

Bioinspired fluorescent nanodots, also known as biodots, is a new class of carbon dots derived from biomolecules or natural sources.[13,20−25] In recent years, biodots have received increasing attention in the field of nanochemistry due to their favorable properties such as excellent aqueous dispersibility,[26] inherent biocompatibility,[27] green synthesis, low cost of production,[28] high chemical and photobleaching resistance,[26] as well as tunable fluorescence.[27] In addition, the ultrasmall size of biodots allows attachment to proteins without steric hindrance, thus minimizing the possibility to disturb the protein's native functions. Furthermore, the use of biomolecules and natural products as precursors in the synthesis of biodots also endows them with good biocompatibility and abundant functionalities inherited from the natural

Received: December 19, 2019
Revised: January 16, 2020

precursors, thus giving a large variety of functional groups on the biodot surfaces, enabling fine-tuning of fluorescence, as well as imparting biorecognition characteristics to biodots.[29] These unique properties of biodots render them particularly suitable as fluorescent labels for proteins or as the sensing probes for biomedical diagnosis.

Notoriously known as a "global burden", diabetes mellitus is a major health concern today with the population of diabetic patients consistently increasing year over year.[30] Large efforts have been put in to develop blood glucose sensors for diabetes diagnosis and glucose monitoring. However, most of the glucose sensors in use are invasive, as they require drawing blood from the patients. Therefore, there have been continuous efforts for the development of sensitive, facile, yet noninvasive glucose sensors that utilize other body fluids such as sweat, saliva, and tears for detection.[31,32] These body fluids can be taken noninvasively and are simpler in composition than blood samples. The main challenge is that the glucose level in these fluids is much lower than in blood, thus requiring the noninvasive glucose sensor to exhibit good sensitivity, selectivity, and a suitable linear range.

Herein, we first studied the biodot−protein conjugation process using several model proteins, including bovine serum albumin (BSA), human serum albumin (HSA), lysozyme (Lys), myoglobin (Mb), human hemoglobin (Hb), and bovine catalase (Cat). The photostability, thermal stability, and pH stability of these protein conjugates were thoroughly characterized and compared with their respective native protein functions. The optimized protein conjugation strategy is then applied to conjugate a selected biodot to a particular enzyme of interest, i.e., glucose oxidase (GOx) for biosensor development. Lastly, the as-developed biodot−GOx conjugate was successfully applied as the sensing probe for glucose detection in a single-step fluorescence "turn-off" enzymatic assay. A side-by-side assay was also performed to highlight the improved sensitivity and detection limit for as-developed biodot−GOx conjugate as compared to covalently conjugated biodot−GOx using EDC/NHS chemistry. This facile one-step assay shows a wide linear range from 25 to 1000 μM, which has been tested for glucose quantification in artificial sweat samples with an excellent recovery rate of 100.5 ± 2.2%.

RESULTS AND DISCUSSION

Linker-free Conjugation of Fluorescent TPdot to Proteins of Interest. We have previously developed a panel of amino acid−polymer biodots with ultrasmall size, excellent fluorescence, photostability, and good biocompatibility.[20] These biodots with a carbon core and a polymeric passivation layer can be quickly conjugated to the protein of interest including bovine serum albumin (BSA), human serum albumin (HSA), and lysosome (Lys), through noncovalent interactions (Figure 1a). The as-formed biodot−protein conjugates are purified by dialysis or ultrafiltration before measuring their final sizes and fluorescence properties. Four types of amino acid−polymer biodots were used for the protein conjugation, using BSA protein as a demonstrative example. Among the tested biodots, the threonine−PEI dots (TPdot) with a hydrodynamic size of 1.1 nm (after ultrafiltration) and a more red-shifted emission at 460 nm was selected for subsequent experiments as it renders the highest fluorescence intensity to the TP−BSA conjugates (Figure S1). Figure 1b shows that each of the as-formed TP−protein conjugates are significantly larger in size than their original protein molecules, indicating

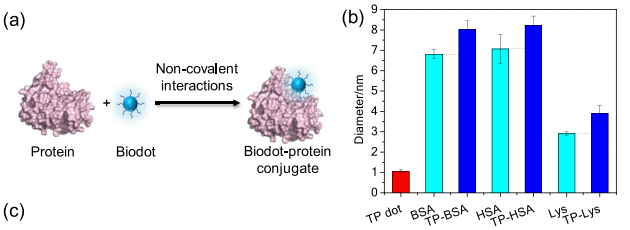

Protein of interest (POI)	Measured protein diameter /nm	TP-protein diameter /nm	Change in diameter /nm
BSA	6.8	8.0	1.2
HSA	7.1	8.2	1.1
Lys	2.9	3.9	1

Figure 1. Schematic illustration of (a) biodot−protein conjugate formation via one-step noncovalent binding interactions. (b) Dynamic light scattering measurements of the hydrodynamic diameter for TPdot, proteins of interest (BSA, HSA, Lys), and the respective TP−protein conjugates. (c) Comparison table showing the increase in hydrodynamic diameter after conjugation.

the successful conjugation of TPdot to the three tested proteins. The increase in hydrodynamic diameters of proteins after conjugation with TPdots is calculated to be around 1 nm, which is about the size of a TPdot. This increase probably indicates half a layer of biodots being conjugated around a protein molecule, suggesting close interactions of TPdots with clefts on the protein surfaces (Figure 1c).

In addition to the hydrodynamic sizes, the fluorescence intensities of the TP−protein conjugates were also measured. Six common proteins with different sizes, shapes, and functions including BSA, HSA, Lys, catalase (Cat), hemoglobin (Hb), and myoglobin (Mb) were tested in this study (Table S1). As shown in Figure 2, TP−BSA, TP−HSA, TP−Lys, and TP−Cat conjugates exhibit relatively high fluorescence intensities, while the fluorescence of TP−Hb and TP−Mb conjugates are only half of that in Figure 2a−d, suggesting strong fluorescence quenching in these two conjugates (Figure 2e,f).

The fluorescence quenching of TPdots in TP−Hb and TP−Mb conjugates is likely due to the inner filter effect contributed by $\pi-\pi$ interactions between TPdots and heme units in hemoglobin and myoglobin.[33,34] On the contrary, the fluorescence of TPdots in TP−cat conjugates remains high due to its deeply buried heme unit within the protein structure preventing effective interactions with the biodots. Upon detailed comparison of the protein structures between hemoglobin, myoglobin, and catalase, it was found that the heme unit in catalase is deeply buried (3−4 Å) inside the bulky protein structure with a narrow pathway (Figure S2a,b) that only allows small molecules to interact with the heme unit.[35] Moreover, hydrophobic residues reside in the entire pathway with hydrophilic residues present at the entrance,[36] which possibly prevent the larger-sized and hydrophilic TPdots from encountering the heme unit for fluorescence quenching. Hemoglobin and myoglobin both exhibit wider pathways for the heme unit (Figure S2c,d).[37−39] Thus, the chances of TPdot encountering the heme unit in both hemoglobin and myoglobin is higher, resulting in significant quenching as compared to TP−catalase conjugates.

Various types of noncovalent interactions contributed to the successful formation of TP−protein conjugates. The ultrafiltered TPdots display a positive zeta potential of 10.5 ± 1.4 mV, indicating that the surface of the TPdots had a net positive charge. Since the isoelectric points (pI) of many proteins are

https://dx.doi.org/10.1021/acs.bioconjchem.9b00856
Bioconjugate Chem. XXXX, XXX, XXX−XXX

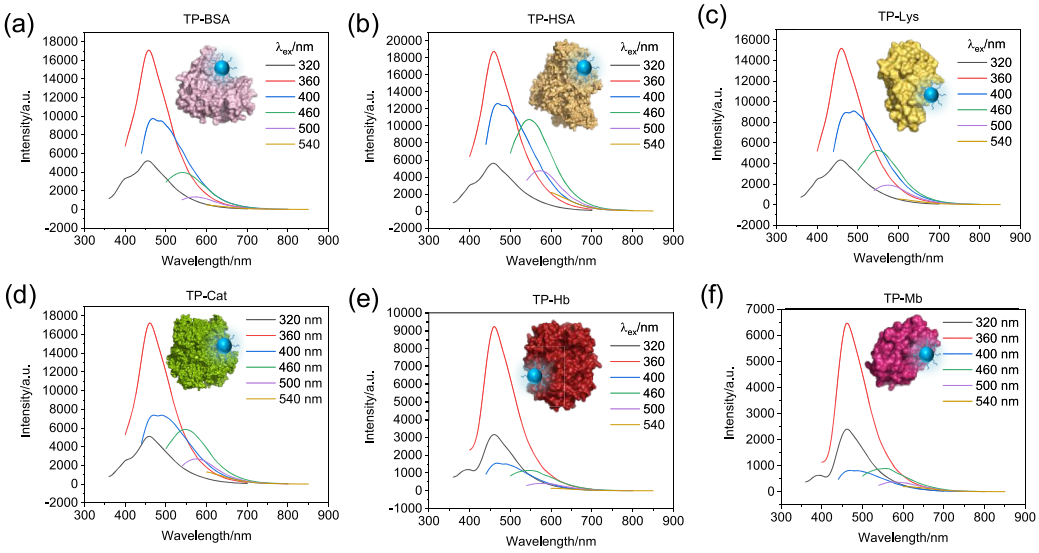

Figure 2. Photoluminescence spectra of the biodot−protein conjugates: (a) TP−BSA, (b) TP-HSA, (c) TP-Lys, (d) TP-Cat (e) TP-Hb, and (f) TP-Mb excited at different wavelengths (λ_{ex}/nm).

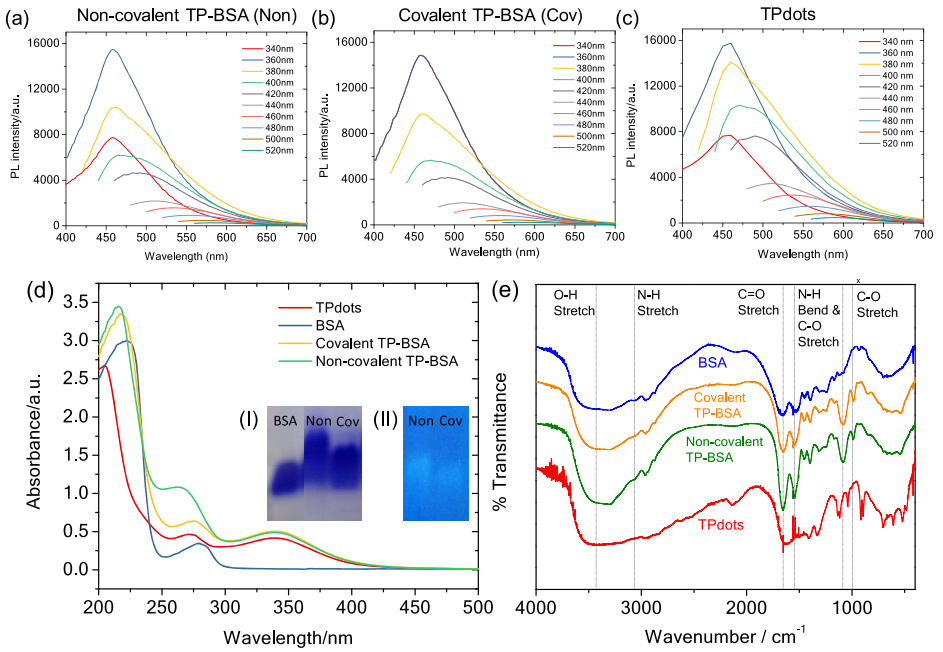

Figure 3. Photoluminescence (PL) spectra of (a) noncovalent TP−BSA conjugates via linker-free route, (b) covalent TP−BSA conjugates via EDC/NHS reaction, and (c) TPdots under UV excitation in the wavelengths from 340 to 520 nm. (d) UV−vis spectra of TPdots, BSA, and TP−BSA conjugates. Insets in (d) show the gel-electrophoresis photographs of the BSA and TP−BSA conjugates formed through noncovalent (Non) and covalent (Cov) methods under (I) white light and (II) UV light at 365 nm; (e) FTIR spectra of TPdots (red), BSA (blue), noncovalent (yellow), and covalent (green) TP−BSA conjugates, respectively.

less than 7 (Table S1), these proteins exhibit a net negative charge at neutral pH. For instance, the zeta potential of BSA is measured to be −16.9 ± 0.7 mV, and the TP−BSA conjugates exhibit a zeta potential of −11.1 ± 0.8 mV. Thus, electrostatic attractions may have been one of the major forces holding the conjugated complex together. However, it is not the only interaction responsible for the stable conjugation, since our TPdots could also be conjugated to lysozymes with a high pI of 11. It is speculated that the (1) $\pi-\pi$ interactions between biodots and the aromatic rings of proteins, (2) hydrogen bonds between hydroxyl, carboxylic, and amine groups in both TPdots and proteins, and (3) dipole−dipole moments between polar groups may also contribute to the overall strength of the noncovalent interactions leading to a stable conjugate formation.

Noncovalent vs Covalent Biodot−Protein Conjugates. We then compared the TP−protein conjugates prepared through the noncovalent interactions to those formed by the conventional covalent conjugation (with the use of chemical linkers EDC and NHS) using BSA as the model protein. The photoluminescence (PL) intensity of the noncovalently conjugated TP−BSA (Figure 3a) is similar to

https://dx.doi.org/10.1021/acs.bioconjchem.9b00856
Bioconjugate Chem. XXXX, XXX, XXX−XXX

that of covalently conjugated TP−BSA (Figure 3b), which corresponds to the PL spectra of TPdots (Figure 3c). These results suggested that the PL properties of TPdots were not altered by the conjugation method. However, it was noticed that the noncovalent TP−BSA conjugates display a slightly smaller hydrodynamic diameter of 7.7 ± 0.3 nm as compared to the covalent TP−BSA conjugates (9.1 ± 0.4 nm). As shown in the UV−vis spectra (Figure 3d), TPdots show three peaks at 205, 271, and 339 nm, respectively. The absorption maximum at 205 nm is attributed to the $\pi-\pi^*$ transition from C═C or C═O groups,[40] while the absorption peaks at 271 and 339 nm wavelength could be attributed to the $n-\pi^*$ transitions.[41,42] On the other hand, BSA typically shows two characteristic peaks at 219 and 279 nm, which correspond to the absorption from the BSA's backbone and the aromatic amino acids, i.e., tryptophan (Trp), tyrosine (Tyr), and phenylalanine (Phe), respectively.[43] Both the noncovalent and covalent TP−BSA conjugates show characteristic peaks of TPdots and BSA, indicating successful protein conjugation using the new linker-free method reported herein.

Furthermore, gel electrophoresis was performed to investigate the biodot−protein conjugation (Figure 3d inset). The protein bands for both noncovalent and covalent TP−BSA conjugates are slightly higher than BSA, indicating that the conjugates have slightly larger molecular weight than BSA alone, which corresponds to our earlier hydrodynamic size measurements in Figure 1b. As shown in Figure 3e, the Fourier-transform infrared spectroscopy (FTIR) fingerprints of TP−BSA include the signature peaks of both TPdots and BSA. The two sharp peaks at around 1090 cm^{-1} (C—O stretching) and 990 cm^{-1} may be attributed to TPdots. On the other hand, BSA displays four signature peaks including a strong, broad peak at around 3600−3200 cm^{-1} attributed to stretching vibration of O—H bond,[44] a medium shoulder peak at 3064 cm^{-1} assigned as amide A band (N—H stretching), a strong peak at 1653 cm^{-1} assignable to amide I band (C═O stretching),[44] and a sharp peak at 1531 cm^{-1} assigned as amide II band (combination of N—H bending and C—N stretching).[44] All four peaks were observed in noncovalent TP−BSA conjugates, confirming successful conjugation.

Stability Studies of Biodot−Protein Conjugates. Upon confirming successful conjugation, we subsequently performed a series of tests to assess stability of the TP−BSA conjugate with respect to continuous UV irradiation, elevated temperature, and change in pH prior to using it as the potential fluorescent probes.

Photostability. Photobleaching experiments with continuous UV irradiation were conducted on TPdot and TP−BSA conjugates respectively to investigate their photostability in aqueous solution. Figure 4a,c shows that the TPdots are intrinsically photostable with less than 5% decrease in PL intensity within the first 2 h of continuous UV irradiation. Nevertheless, the photostability of noncovalent TP−BSA conjugate also followed the same trend as TPdots alone, suggesting its suitability to be used as the fluorescence sensing probe for glucose detection, which only requires minutes to complete. However, its intensity drops sharply after 2.5 h, suggesting severe aggregation with visible precipitation as observed at the end of prolonged UV irradiation. It is noteworthy to point out that the noncovalent TP−BSA conjugates reported here are proven to be more photostable as compared to the conventional organic fluorophores (FITC)-conjugated proteins in the first 2.5 h of irradiation (Figure 4d).

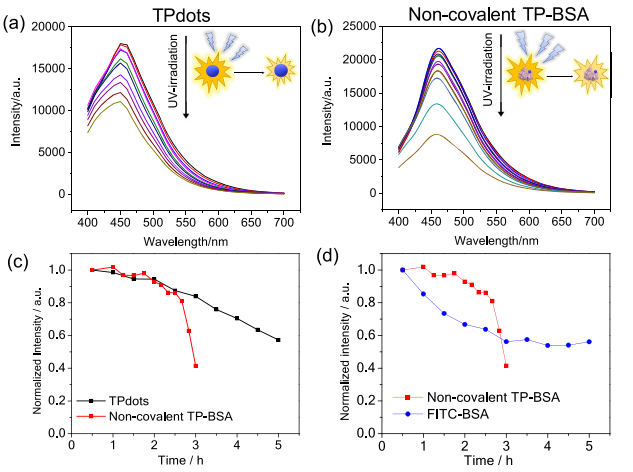

Figure 4. Photoluminescence (PL) spectra of (a) TPdots and (b) TP−BSA conjugates at different time points under 360 nm excitation. Overlay of the maximum PL intensities of the (c) TPdots vs noncovalent TP−BSA conjugates and (d) noncovalent TP−BSA vs FITC-BSA conjugates over time (0−5 h), respectively.

When comparing the PL intensity remaining after 30 min UV irradiation, both noncovalently and covalently conjugated TP−BSAs are considered to be photostable (Figure S3a). As PL measurement is usually completed within minutes, the photostability of TP−BSA is sufficient for a fluorescence biosensor operation. Furthermore, the hydrodynamic diameters of TP−BSA conjugates remained constant upon UV irradiation (30 min), indicating that the TP−protein complex is structurally stable within 30 min (Figure S3b).

Thermal Stability. In addition to photostability, it is also important to investigate the thermal stability of the biodot−protein conjugates to ensure their structural stability and proper functions. As shown in Figure 5a,b, there is no change in the photoluminescence (PL) intensity of the as-prepared TP−BSA and TP−HSA conjugates. The hydrodynamic sizes of the protein alone and TP−protein conjugates were also measured over this temperature range, in order to determine their respective thermal stabilities. The melting temperatures (T_m) of proteins and their TP−protein conjugates were also determined from the onset of size change.[45] It is found that the overall size changes of the TP−BSA (Figure 5c) and TP−HSA (Figure 5d) conjugates are much larger than that of the BSA and HSA proteins alone. However, the observed T_m values are higher for both TP−protein conjugates as compared to the proteins alone, suggesting the stabilization effect of the TPdots in the conjugates.

Comparing the thermal stability of noncovalent and covalent TP−BSA conjugates, it is observed from Figure 5e that the PL values of both types of protein conjugates do not change significantly as the temperature increases from 23 to 95 °C. On the other hand, the hydrodynamic diameters of the covalent TP−BSA conjugates remain constant up to 65 °C, whereas the noncovalent TP−BSA only show sharp size increase above 75 °C (Figure 5f), which is an indication of protein denaturation due to irreversible aggregation above melting temperature (T_m). This data suggests the noncovalent TP−BSA conjugates are more thermally stable than the covalent TP−BSA conjugates.

pH Stability and Long-Term Storage Stability. As for the pH stability, both the covalent TP−BSA and noncovalent TP−

https://dx.doi.org/10.1021/acs.bioconjchem.9b00856
Bioconjugate Chem. XXXX, XXX, XXX−XXX

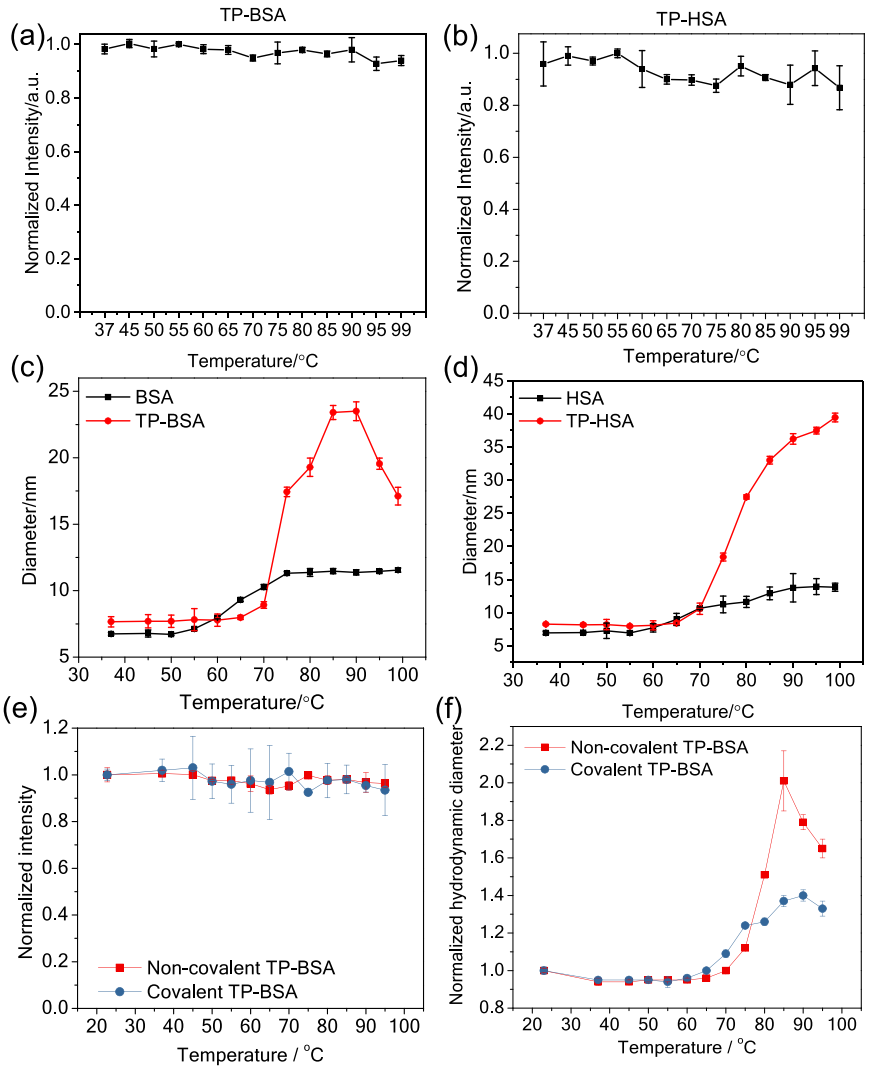

Figure 5. Normalized PL intensities of noncovalent (a) TP−BSA and (b) TP−HSA conjugates with increasing temperatures. Hydrodynamic diameters of (c) BSA and (d) HSA proteins vs their respective conjugates at increasing temperatures. (e) Normalized PL intensity and (f) hydrodynamic diameter after 10 min incubation at increasing temperatures for noncovalent (red) vs covalent (blue) TP−BSA conjugates.

BSA conjugates are stable over the physiological neutral range (pH 6−8) as shown in Figure S3c, where a significantly higher photoluminescence (PL) intensity was observed in acidic medium (Figure S3d) similar to other PEI-passivated dots reported in the literature.[46] This is due to the nature of PEI polymers used to passivate the TPdots with abundant amine functional groups, exhibiting strong electron donating ability. In the basic medium, amine groups can transfer electrons to the core fluorescent units, thus decreasing the overall PL intensity, whereas protonation of the amine groups under acidic conditions eliminates the electron transfer leading to higher PL intensity. Trends in hydrodynamic diameter of the conjugates were generally similar to the trend of BSA in different pH media as reported by Kvasnov et al.[47] Collectively, these results indicate that the stabilities of noncovalent TP−BSA conjugates were highly similar to that of covalent TP−BSA at physiological pH, suggesting that the linker-free conjugation method is an effective way to develop fluorescent-labeled protein probes for biosensing applications.

The stability of proteins against aggregation when stored over prolonged periods is crucial for their utility, especially for the therapeutic proteins.[48] Over 30% of FDA-approved drugs are protein therapeutics,[49] and the need for protein stabilization is significant. As such, the size and fluorescence of TP−protein conjugates were tested over prolonged storage at room temperature and 4 °C, respectively. According to Figure S4, the size and PL intensity remained unchanged up until 20 days of storage at these conditions, indicating the possibility of utilizing TPdots for the protein stabilization. Furthermore, we continued to monitor the noncovalent and covalent TP−BSA samples and found that both samples are stable for up to four months (Figure S5).

Protein Functionality Studies. Besides structural characterizations, it is also critical for the as-formed protein conjugate to preserve its native functions such as drug binding and enzymatic activities demonstrated in this study.

Drug Binding Activity. The stability of proteins toward aggregation is crucial for drug delivery systems.[50] Thermal stability experiments were conducted on drug-bound proteins and their conjugates to determine whether the drug binding activity of the protein is retained after conjugation. Both ibuprofen- and warfarin-bound proteins were more stable than

https://dx.doi.org/10.1021/acs.bioconjchem.9b00856
Bioconjugate Chem. XXXX, XXX, XXX−XXX

the proteins alone, and drug-bound TP−protein conjugate shows similar stability to drug-bound protein (Figure 6). The

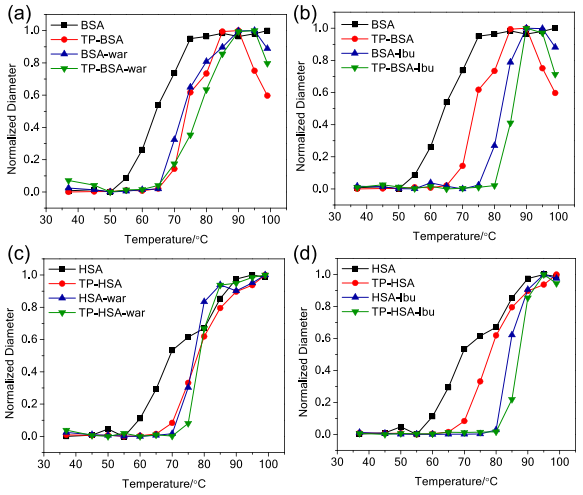

Figure 6. Effect of temperature on the hydrodynamic diameter of (a,b) BSA, TP−BSA conjugates with drug binding: (a) BSA−warfarin, TP−BSA−warfarin; (b) BSA-ibuprofen, TP−BSA−ibuprofen; and (c,d) HSA, TP−HSA conjugates with drug binding: (c) HSA−warfarin, TP−HSA−warfarin, (d) HSA−ibuprofen, TP−HSA−ibuprofen.

T_m of protein−drug is comparable to that of TP−protein−drug, proving that the TPdot conjugation does not influence the protein−drug interactions. This suggests that TPdot could have been conjugated at locations away from the drug binding sites on the proteins or the binding affinity of TPdots to the proteins is lower than the drug molecules, thus protein−drug binding will dominate due to stronger competition.

Enzymatic Activity. As many proteins possess enzymatic functions, the effect of TPdot conjugation on the enzymatic activity of proteins was also investigated. Lysozyme is a bacteriolytic agent, which cleaves glycosidic bonds in the bacteria cell wall.[51] A known method of determining lysozyme activity is through the lysis of *Micrococcus lysodeikticus* (M.l.) cells, whereby the destruction of the cell walls results in decreased absorbance for the lysed cells as compared to the intact cells. The rate of absorbance decrease correlates proportionally to the lysozyme activity. As shown in Figure S6, the absorbance values of both TP−Lys and lysozyme treated samples decrease at a similar rate, indicating that the enzymatic activity of lysozyme was not affected by the noncovalent conjugation. It is postulated that the ultrasmall TPdots were either conjugated on the binding sites far away from the active site of lysozyme or weakly conjugated near the binding site via the noncovalent modes of binding, allowing the enzymatic activity of conjugated protein to remain intact.

Noncovalent TP−GOx Conjugates as Sensing Probes for Sweat Glucose Quantification. The structural and functional characterizations of TP−BSA conjugates have shown good stability and retained functionality of the as-formed conjugates as suitable probes for biosensing applications. Therefore, we conjugated the TPdots to a widely used enzyme glucose oxidase (GOx) and applied the TP−GOx conjugates for glucose quantification in sweat samples.

Assay Development. The principle of the glucose sensing assay is depicted in Figure 7a. Glucose oxidase is an enzyme that catalyzes the reaction between D-glucose, water, and oxygen to produce hydrogen peroxide and D-glucono-1,5-lactone. The as-produced hydrogen peroxide can then react with the added Fe^{2+} to produce hydroxyl radical, hydroxide,

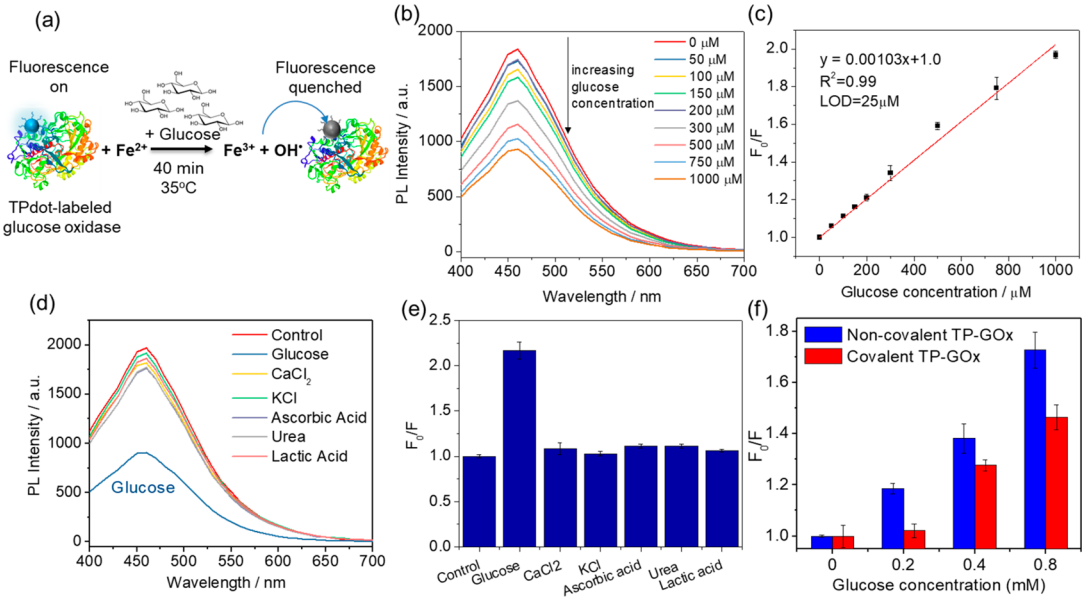

Figure 7. (a) One-step glucose assay using TP−GOx conjugates as enzymatic fluorescent sensing probe. (b) Average PL spectra of TP−GOx excited at 360 nm wavelength in the presence of Fe^{2+} after incubation with different concentrations of glucose (25−1000 μM). (c) Corresponding calibration plot of F_0/F (relative fluorescence intensity before and after addition of artificial sweat sample) against increasing glucose concentrations. (d) PL spectra of TP−GOx conjugates in the presence of common interference compounds. (e) Interference study showing the quenching abilities (F_0/F) of other compounds frequently present in human sweat. Error bars represent standard deviations for triplicate measurements. (f) Side-by-side glucose detection assay confirming the improvement in sensitivity and the detection limit for the noncovalently conjugated TP−GOx via linker-free route vs covalently conjugated TP−GOx using EDC/NHS.

https://dx.doi.org/10.1021/acs.bioconjchem.9b00856
Bioconjugate Chem. XXXX, XXX, XXX−XXX

and Fe^{3+} via Fenton reaction.[52] Since hydroxyl radicals and Fe^{3+} ions are able to quench fluorescent nanoparticles such as carbon dots,[53] the TP−GOx/Fe^{2+} system is used to develop a fluorescence "turn-off" assay for glucose quantification.

The representative PL spectra were plotted in Figure 7b showing the gradual fluorescence quenching of TP−GOx conjugates as the concentration of glucose increases. The calibration plot in Figure 7c shows that the linear range is from 25 to 1000 μM, which covers the glucose concentration levels in human sweat. In this single-step assay, the hydroxyl radicals and Fe^{3+} were immediately available to quench TP−GOx conjugates in close proximity. The limit of detection (LOD) was calculated to be 25 μM, which is sufficient for sweat glucose sensing. In summary, our probe offers a wider linear range with good sensitivity as compared to the other reported fluorescent probes for glucose detection (Table S2). Interference study was further conducted to examine the effect of other substances commonly present in sweat, such as Ca^{2+}, K^+, Cl^-, ascorbic acid, urea, and lactic acid (Figure 7d,e). Negligible interference was observed from these common constituents of sweat.

We further compared the performance of the noncovalently conjugated TP−GOx as developed in this study to the covalent TP−GOx conjugates in a side-by-side assay for glucose detection (Figure 7f). Results show that the noncovalent TP−GOx sensing probes give higher F_0/F ratio than those prepared by covalent EDC/NHS method at all the concentrations tested. In addition, the noncovalent TP−GOx displays a distinct difference at 0.2 mM glucose, whereas the fluorescent signal for covalent TP−GOx at 0.2 mM is not distinguishable from the 0 mM negative control. It is obvious that the noncovalent TP−GOx could achieve better assay performance than the covalent TP−GOx in terms of assay sensitivity and detection limit, hinting the better preservation of native protein functions through the noncovalent method reported herein.

Glucose Detection in Artificial Sweat. The linear range of the optimized one-step assay is 25 to 1000 μM, which well covers the reported level of sweat glucose for the healthy (60−110 μM) and diabetic individuals (100−1000 μM).[54,55] In this study, the artificial sweat samples were spiked in with 400 μM of glucose. Control sweat sample without glucose spiked-in was also measured to provide a baseline for the calculation of the relative fluorescence intensity (F_0/F) which is an indicative measure of the quenching extent. The detection mixture containing TP−GOx, Fe^{2+}, and sweat samples was incubated for 40 min at 35 °C and subjected to PL measurement. The concentration of glucose detected from the artificial sweat samples (in quadruplicates) ranged from 393 to 414 μM according to our calibration. The average concentration of glucose detected from the artificial sweat samples was 402 ± 9 μM. When we compared the detected glucose concentration to the original spiked-in glucose concentration, we obtained remarkable recovery rate of 100.5 ± 2.2% (Table 1), showing the high accuracy of this one-step assay for quantifying the unknown concentration of glucose in artificial sweat.

Table 1. Determination of Glucose Concentration from Artificial Sweat

artificial sweat sample	F_0/F	glucose concentration detected/μM	glucose spiked-in/ μM	recovery rate/%
1	1.405	393	400	98.3
2	1.412	400	400	100.0
3	1.413	401	400	100.3
4	1.426	414	400	103.5
Average	1.414 ± 0.01	402 ± 9	400	100.5 ± 2.2

CONCLUSIONS

In summary, several model proteins were used to demonstrate that biodots derived from an amino acid and cationic polymer could effectively label various proteins through noncovalent conjugation without the addition of any chemical linkers. The resultant biodot−protein conjugates exhibit similar photostability and thermal stability as that of covalent biodot−protein conjugates prepared using chemical linkers (e.g., EDC/NHS). We also observed that the noncovalent TP−BSA conjugates are stable over the physiological range of pH, i.e., at pH of 6−8. The noncovalent conjugation method was applied to prepare the biodot−GOx conjugates as a fluorescent sensing probe for sweat glucose detection. A wide linear range of 25−1000 μM and a low LOD of 25 μM were achieved for the one-step enzymatic fluorescent "turn-off" assay. Improved sensitivity and detection limit were observed for glucose assay using our noncovalent biodot−GOx conjugates as compared to the covalent conjugates through a side-by-side assay. Furthermore, the TP−GOx probe is highly selective for glucose detection with negligible interference from other common sweat metabolites. Finally, glucose concentration was successfully determined in complex artificial sweat samples using the optimized assay, achieving a remarkable recovery rate of 100.5 ± 2.2%, which indicates its high potential for real-life application of sweat glucose detection. This work has demonstrated a linker-free method in preparing noncovalent biodot−protein conjugates with improved stability and well-preserved protein functions, which has laid the groundwork for utilizing such noncovalent biodot−enzyme conjugates for simple and accurate diseases diagnosis, e.g., sweat glucose detection in complex samples.

EXPERIMENTAL SECTION

Chemicals and Reagents. We have previously developed a panel of amino acid−polymer L-serine, L-threonine, branched polyethylenimine (PEI), chitosan, histamine dihydrochloride (99%), bovine serum albumin (BSA), human serum albumin (HSA), lysozyme from chicken egg (Lys), myoglobin from equine skeletal muscle (Mb), hemoglobin from human (Hb), catalase from bovine liver (Cat), glucose oxidase from *Aspergillus niger* (GOx), ibuprofen, warfarin, 1-ethyl-3-(3-(dimethylamino)propyl)carbodiimide (EDC), *n*-hydroxysuccinimide (NHS), D-glucose, hydrogen peroxide, sodium acetate, 1 M phosphate buffer saline (PBS, pH = 7.4), fluorescein isothiocyanate (FITC), and agarose were purchased from Sigma-Aldrich. Proteins were dissolved in phosphate-buffered saline (PBS) and filtered through 0.22 μm filter before use.

Measurements. Tecan Infinite M200 plate reader was used to measure the fluorescence spectra (excitation wavelength: 360 nm, Gain: 75, step size: 10 nm). Wyatt DynaPro PlateReader-II was used for hydrodynamic diameter measurements. Shimadzu UV-2450 UV−vis spectrophotometer was used for absorbance measurement in the 200−800 nm range. The Fourier transform infrared (FTIR) spectroscopic measurement was carried out using PerkinElmer Fourier transform infrared spectrometer. Thermo Scientific Orion Star A111 Benchtop pH meter was used for pH measurements. Zeta

https://dx.doi.org/10.1021/acs.bioconjchem.9b00856
Bioconjugate Chem. XXXX, XXX, XXX−XXX

potential measurements were performed using Malvern Zetasizer.

Synthesis of Biodots. Threonine−PEI biodots (TPdots) was hydrothermally synthesized as published previously[20] with modifications. Briefly, threonine and PEI were mixed at a 2:1 ratio and completely dissolved in ultrapure water before transferring to a Teflon autoclave and heated at 180 °C for 24 h in Memmert Universal Oven (UF55). The reaction product was first purified by centrifugation and dialysis. The purified sample was ultrafiltered using a membrane filter with molecular weight cut-off (MWCO) of 3000 Da at 8000 rpm for 10 min (min), and the filtrate was collected to obtain ultrasmall TPdots for protein conjugation.

Biodot−Protein Conjugation. For noncovalent conjugation of biodot−protein, protein of interest was first weighed and dissolved in 10 mM PBS. Both protein and biodot solutions were filtered through a 0.22 μm filter prior to mixing. An optimized weight ratio of protein and biodot (1:5) was mixed in 10 mM PBS buffer for 2 h (h) with constant stirring. For the preparation of TP−GOx conjugate, GOx was first dissolved in 50 mM sodium acetate buffer (pH 5.0) and then mixed with TPdot solution at 1:5 ratio for 2 h with stirring.

For covalent conjugation of TP−BSA and TP−GOx, BSA was activated with EDC and NHS in 1:5:10 molar ratio for 15 min in MES buffer with 0.5 M NaCl (pH 6). Excess EDC and NHS were removed via ultrafiltration at 8000 rpm for 10 min and the buffer was exchanged to 10 mM PBS. Then, the activated BSA or GOx was stirred with TPdot at 1:5 w/w ratio for 2 h.

As-formed TP−protein conjugates were purified via ultrafiltration using a membrane filter (MWCO: 3000 Da) at 8000 rpm for 10 min. The filtrate was removed and the centrifugation unit was topped up with 10 mM PBS (200 μL), and the ultrafiltration process was repeated two more times to obtain purified TP−protein conjugates.

Characterization of Biodot−Protein Conjugates. *Photostability Study.* TP−BSA solution was irradiated with UV light at 365 nm wavelength for 5 h. The fluorescence intensity and the hydrodynamic diameter of the sample were measured at 30 min intervals.

Thermal Stability and Protein Melting Point Study. TP−BSA samples were filtered by 0.22 μm syringe filter prior to the study. Proteins (BSA, HSA, Lys), biodot−protein conjugates (TP−BSA, TP−HSA, TP−Lys), and drug-bound biodot−protein conjugates (TP−BSA−warfarin, TP−BSA−ibuprofen, TP−HSA−warfarin, TP−HSA−ibuprofen) were heated to various temperatures (37, 45, 50, 55, 60, 65, 70, 75, 80, 85, 90, 95, 99 °C) and maintained for 10 min on an Eppendorf Thermomixer with 300 rpm shaking.

pH Stability Study. TP−BSA solutions were adjusted to various pH with 0.1 M HCl or 0.1 M NaOH. The solutions were left to stand for 30 min at room temperature before taking measurements.

Drug Binding Study. All samples were filtered by a 0.22 μm syringe filter prior to the study. 1 μL of 0.45 M warfarin in DMSO or ibuprofen in 100% ethanol was mixed with 200 μL of protein or TP−protein solution at room temperature for 1 h. Thermal stability experiments were subsequently conducted as described above.

Enzyme Activity Study. *Micrococcus lysodeikticus* (M.L.) powder was suspended in 10 mM PBS (pH 6.24) to obtain a final concentration of 0.15 mg/mL. 100 μL of M.L. suspension was mixed with 1.5 μL of TP-Lys or lysozyme in a 96-well plate. The absorption intensity at 450 nm wavelength was measured at 1 min intervals.

Glucose Detection. *One-Step Assay for Glucose Quantification.* All the reagents and TP−GOx were prepared in 50 mM sodium acetate buffer (pH = 5.0). An optimized amount of TP−GOx (25 μL, 0.1 mg/mL, pH = 5.5), glucose solution (25 μL), and $FeSO_4$ solution (25 μL,7.5 mM) were directly mixed in sodium acetate buffer (50 μL), and was placed in a thermomixer set at 35 °C and 300 rpm. D-Glucose concentrations from 0 to 1000 μM were used for the assay. The Fe^{2+} concentration was kept constant at 1500 μM, following the Fe^{2+}:H_2O_2 ratio of 1.5 based on maximum concentration of glucose. After incubation for specified durations, the mixture was pipetted into a microplate for fluorescence measurement.

Interference Study. For interference study, the same procedures for one-step assay were followed. The final concentrations of glucose and all the other reagents including Ca^{2+}, K^+, Cl^-, ascorbic acid, urea, and lactic acid were 1.0 mM.

Glucose Quantification in Artificial Sweat. Artificial sweat solution was prepared according to ISO standards (pH 5.5) with modifications.[56] Briefly, sodium chloride (250 mg), L-histidine (18.7 mg), and anhydrous sodium dihydrogen orthophosphate (84.6 mg) were dissolved in ultrapure water (40 mL), then the pH was adjusted to 5.5 with 0.1 M HCl (390 μL). The solution was made up to 50 mL with ultrapure water. Glucose-spiked (2.0 mM) artificial sweat was prepared by dissolving D-glucose (9 mg) in artificial sweat solution (25 mL).

For quantification of glucose in artificial sweat, noncovalent TP−GOx (25 μL, 0.1 mg/mL, pH = 5.0), artificial sweat (25 μL, pH = 5.5), iron(II) sulfate (25 μL, pH = 5.0), and 50 mM sodium acetate buffer (50 μL, pH = 5.0) were mixed. The tube was incubated in a thermomixer at 35 °C and 300 rpm for 40 min. The sample were cooled for 5 min and the fluorescence spectra from 400 to 700 nm were measured with excitation at 360 nm.

■ ASSOCIATED CONTENT

Supporting Information

The Supporting Information is available free of charge at https://pubs.acs.org/doi/10.1021/acs.bioconjchem.9b00856.

Comparison of four types of biodots; Physical properties of proteins used in this study; Schematic of heme site in catalase, hemoglobin, and myoglobin; Photostability and pH stability study of noncovalent vs covalent TP−BSA conjugates; Size and PL stability of TP−BSA, TP-HSA, and TP-Lys conjugates over 20 days; Long-term stability of noncovalent vs covalent TP−BSA conjugates; Maintenance of enzymatic activity in TP-Lys conjugates; Comparison of fluorescent glucose sensor performances (PDF)

■ AUTHOR INFORMATION

Corresponding Authors

Xin Ting Zheng − *Agency for Science, Technology and Research (A*STAR), Institute of Materials Research and Engineering (IMRE), Singapore 138634 Singapore;* orcid.org/0000-0002-1431-0929; Email: zhengxt@imre.a-star.edu.sg

Yen Nee Tan − *Agency for Science, Technology and Research (A*STAR), Institute of Materials Research and Engineering (IMRE), Singapore 138634 Singapore; Faculty of Science,*

https://dx.doi.org/10.1021/acs.bioconjchem.9b00856
Bioconjugate Chem. XXXX, XXX, XXX−XXX

Agriculture & Engineering, Newcastle University, Newcastle Upon Tyne NE1 7RU, United Kingdom; Department of Chemistry, National University of Singapore, Singapore 117543 Singapore; orcid.org/0000-0002-4003-063X; Email: yennee.tan@ncl.ac.uk

Authors

Yoonah Choi − *Department of Chemistry, National University of Singapore, Singapore 117543 Singapore*

Darren Guan Ge Phua − *Department of Chemistry, National University of Singapore, Singapore 117543 Singapore;* orcid.org/0000-0002-2621-4010

Complete contact information is available at: https://pubs.acs.org/10.1021/acs.bioconjchem.9b00856

Notes

The authors declare no competing financial interest.

■ ACKNOWLEDGMENTS

This work is financially supported by the Institute of Materials Research and Engineering (IMRE), Agency for Science, Technology and Research (A*STAR), Singapore, under the Biomimetic and Biomedical Program exploratory fund IMRE/16-1P1401. The authors acknowledge the support from IMRE, National University of Singapore, and Newcastle University for the collaborative research.

■ REFERENCES

(1) Tantama, M., Hung, Y. P., and Yellen, G. (2011) Imaging Intracellular pH in Live Cells with a Genetically Encoded Red Fluorescent Protein Sensor. *J. Am. Chem. Soc. 133*, 10034−10037.

(2) Lai, Y. T., Chang, Y. Y., Hu, L., Yang, Y., Chao, A., Du, Z. Y., Tanner, J. A., Chye, M. L., Qian, C., Ng, K. M., et al. (2015) Rapid labeling of intracellular His-tagged proteins in living cells. *Proc. Natl. Acad. Sci. U. S. A. 112*, 2948−53.

(3) Zhang, Z., Smith, B. A., Wang, L., Brock, A., Cho, C., and Schultz, P. G. (2003) A new strategy for the site-specific modification of proteins in vivo. *Biochemistry 42*, 6735−6746.

(4) Fernández-Suárez, M., Baruah, H., Martínez-Hernández, L., Xie, K. T., Baskin, J. M., Bertozzi, C. R., and Ting, A. Y. (2007) Redirecting lipoic acid ligase for cell surface protein labeling with small-molecule probes. *Nat. Biotechnol. 25*, 1483.

(5) Geng, J., Goh, W. L., Zhang, C., Lane, D. P., Liu, B., Ghadessy, F., and Tan, Y. N. (2015) A highly sensitive fluorescent light-up probe for real-time detection of the endogenous protein target and its antagonism in live cells. *J. Mater. Chem. B 3*, 5933−5937.

(6) Yu, Y., Geng, J., Ong, E. Y. X., Chellappan, V., and Tan, Y. N. (2016) Bovine Serum Albulmin Protein-Templated Silver Nanocluster (BSA-Ag13): An Effective Singlet Oxygen Generator for Photodynamic Cancer Therapy. *Adv. Healthcare Mater. 5*, 2528−2535.

(7) Yu, Y., New, S. Y., Lin, J., Su, X., and Tan, Y. N. (2015) A Rapid and Quantitative Fluorimetric Method for Protein-Targeting Small Molecule Drug Screening. *J. Visualized Exp.*, No. e53261.

(8) Yu, Y., New, S. Y., Xie, J., Su, X., and Tan, Y. N. (2014) Protein-based fluorescent metal nanoclusters for small molecular drug screening. *Chem. Commun. 50*, 13805−13808.

(9) Gao, X., Cui, Y., Levenson, R. M., Chung, L. W. K., and Nie, S. (2004) In vivo cancer targeting and imaging with semiconductor quantum dots. *Nat. Biotechnol. 22*, 969.

(10) Lu, Z., Zhu, Z., Zheng, X., Qiao, Y., Guo, J., and Li, C. M. (2011) Biocompatible fluorescence-enhanced ZrO2−CdTe quantum dot nanocomposite for in vitro cell imaging. *Nanotechnology 22*, 155604.

(11) Chen, J., Than, A., Li, N., Ananthanarayanan, A., Zheng, X., Xi, F., Liu, J., Tian, J., and Chen, P. (2017) Sweet graphene quantum dots for imaging carbohydrate receptors in live cells. *FlatChem. 5*, 25−32.

(12) Yang, M., Javadi, A., and Gong, S. (2011) Sensitive electrochemical immunosensor for the detection of cancer biomarker using quantum dot functionalized graphene sheets as labels. *Sens. Actuators, B 155*, 357−360.

(13) Choi, Y., Zheng, X. T., and Tan, Y. N. (2020) Bioinspired carbon dots (biodots): emerging fluorophores with tailored multiple functionalities for biomedical, agricultural and environmental applications. *Mol. Syst. Des. Eng. 5*, 67−90.

(14) Srinivasan, K., Subramanian, K., Murugan, K., and Dinakaran, K. (2016) Sensitive fluorescence detection of mercury(ii) in aqueous solution by the fluorescence quenching effect of MoS2 with DNA functionalized carbon dots. *Analyst 141*, 6344−6352.

(15) Kumari, S., Solanki, A., Mandal, S., Subramanyam, D., and Das, P. (2018) Creation of Linear Carbon Dot Array with Improved Optical Properties through Controlled Covalent Conjugation with DNA. *Bioconjugate Chem. 29*, 1500−1504.

(16) Ostadhossein, F., Vulugundam, G., Misra, S. K., Srivastava, I., and Pan, D. (2018) Chirality Inversion on the Carbon Dot Surface via Covalent Surface Conjugation of Cyclic α-Amino Acid Capping Agents. *Bioconjugate Chem. 29*, 3913−3922.

(17) Seo, J., Lee, J., Lee, C. B., Bae, S. K., and Na, K. (2019) Nonpolymeric pH-Sensitive Carbon Dots for Treatment of Tumor. *Bioconjugate Chem. 30*, 621−632.

(18) Sunasee, R., and Narain, R. (2014) *Chemistry of Bioconjugates*, pp 3−75, Wiley Online Books.

(19) Steen Redeker, E., Ta, D. T., Cortens, D., Billen, B., Guedens, W., and Adriaensens, P. (2013) Protein Engineering For Directed Immobilization. *Bioconjugate Chem. 24*, 1761−1777.

(20) Zheng, X. T., and Tan, Y. N. (2019) Development of Blood-Cell-Selective Fluorescent Biodots for Lysis-Free Leukocyte Imaging and Differential Counting in Whole Blood. *Small 0*, 1903328.

(21) Zheng, X. T., Lai, Y. C., and Tan, Y. N. (2019) Nucleotide-derived theranostic nanodots with intrinsic fluorescence and singlet oxygen generation for bioimaging and photodynamic therapy. *Nanoscale Adv. 1*, 2250−2257.

(22) Xu, H. V., Zheng, X. T., Zhao, Y., and Tan, Y. N. (2018) Uncovering the Design Principle of Amino Acid-Derived Photoluminescent Biodots with Tailor-Made Structure−Properties and Applications for Cellular Bioimaging. *ACS Appl. Mater. Interfaces 10*, 19881−19888.

(23) Xu, H. V., Zheng, X. T., Wang, C., Zhao, Y., and Tan, Y. N. (2018) Bioinspired Antimicrobial Nanodots with Amphiphilic and Zwitterionic-like Characteristics for Combating Multidrug-Resistant Bacteria and Biofilm Removal. *ACS Appl. Nano Mater. 1*, 2062−2068.

(24) Zheng, X. T., Xu, H. V., and Tan, Y. N. (2017) Bioinspired Design and Engineering of Functional Nanostructured Materials for Biomedical Applications, in *Advances in Bioinspired and Biomedical Materials*, pp 123−152, Vol. 2, American Chemical Society.

(25) Xu, H. V., Zhao, Y., and Tan, Y. N. (2019) Nanodot-Directed Formation of Plasmonic-Fluorescent Nanohybrids toward Dual Optical Detection of Glucose and Cholesterol via Hydrogen Peroxide Sensing. *ACS Appl. Mater. Interfaces 11*, 27233−27242.

(26) Wang, Y., and Hu, A. (2014) Carbon quantum dots: synthesis, properties and applications. *J. Mater. Chem. C 2*, 6921.

(27) Roy, P., Chen, P.-C., Periasamy, A. P., Chen, Y.-N., and Chang, H.-T. (2015) Photoluminescent carbon nanodots: synthesis, physicochemical properties and analytical applications. *Mater. Today 18*, 447−458.

(28) Wang, Y., Zhu, Y., Yu, S., and Jiang, C. (2017) Fluorescent carbon dots: rational synthesis, tunable optical properties and analytical applications. *RSC Adv. 7*, 40973−40989.

(29) Jelinek, R. (2017) Carbon-Dot Synthesis, in *Carbon Quantum Dots*, pp 5−27, Springer International Publishing, Cham.

(30) Jaacks, L. M., Siegel, K. R., Gujral, U. P., and Narayan, K. M. (2016) Type 2 diabetes: A 21st century epidemic. *Best Pract Res. Clin Endocrinol Metab 30*, 331−43.

(31) Bruen, D., Delaney, C., Florea, L., and Diamond, D. (2017) Glucose Sensing for Diabetes Monitoring: Recent Developments. *Sensors 17*, 1866.
(32) Corrie, S. R., Coffey, J. W., Islam, J., Markey, K. A., and Kendall, M. A. F. (2015) Blood, sweat, and tears: developing clinically relevant protein biosensors for integrated body fluid analysis. *Analyst 140*, 4350−4364.
(33) Bui, T. T., and Park, S.-Y. (2016) A carbon dot−hemoglobin complex-based biosensor for cholesterol detection. *Green Chem. 18*, 4245−4253.
(34) Barati, A., Shamsipur, M., and Abdollahi, H. (2015) Hemoglobin detection using carbon dots as a fluorescence probe. *Biosens. Bioelectron. 71*, 470−475.
(35) Santoni, E., Jakopitsch, C., Obinger, C., and Smulevich, G. (2004) Comparison between catalase-peroxidase and cytochrome c peroxidase. The role of the hydrogen-bond networks for protein stability and catalysis. *Biochemistry 43*, 5792−5802.
(36) Reid, T. J., Murthy, M., Sicignano, A., Tanaka, N., Musick, W., and Rossmann, M. (1981) Structure and heme environment of beef liver catalase at 2.5 A resolution. *Proc. Natl. Acad. Sci. U. S. A. 78*, 4767−4771.
(37) Milani, M., Pesce, A., Ouellet, Y., Ascenzi, P., Guertin, M., and Bolognesi, M. (2001) Mycobacterium tuberculosis hemoglobin N displays a protein tunnel suited for O2 diffusion to the heme. *EMBO J. 20*, 3902−3909.
(38) Kuntz, I. D., Blaney, J. M., Oatley, S. J., Langridge, R., and Ferrin, T. E. (1982) A geometric approach to macromolecule-ligand interactions. *J. Mol. Biol. 161*, 269−288.
(39) Wittenberg, J. B., Bolognesi, M., Wittenberg, B. A., and Guertin, M. (2002) Truncated hemoglobins: a new family of hemoglobins widely distributed in bacteria, unicellular eukaryotes and plants. *J. Biol. Chem. 277*, 871−874.
(40) Choi, Y., Thongsai, N., Chae, A., Jo, S., Kang, E. B., Paoprasert, P., Park, S. Y., and In, I. (2017) Microwave-assisted synthesis of luminescent and biocompatible lysine-based carbon quantum dots. *J. Ind. Eng. Chem. 47*, 329−335.
(41) Xu, H. V., Zheng, X. T., Zhao, Y., and Tan, Y. N. (2018) Uncovering the Design Principle of Amino Acid-Derived Photoluminescent Biodots with Tailor-Made Structure-Properties and Applications for Cellular Bioimaging. *ACS Appl. Mater. Interfaces 10*, 19881−19888.
(42) Wang, W., Damm, C., Walter, J., Nacken, T. J., and Peukert, W. (2016) Photobleaching and stabilization of carbon nanodots produced by solvothermal synthesis. *Phys. Chem. Chem. Phys. 18*, 466−475.
(43) Xu, H., Yao, N., Xu, H., Wang, T., Li, G., and Li, Z. (2013) Characterization of the Interaction between Eupatorin and Bovine Serum Albumin by Spectroscopic and Molecular Modeling Methods. *Int. J. Mol. Sci. 14*, 14185−14203.
(44) Grdadolnik, J., and Marchal, Y. (2001) Bovine Serum Albumin Observed by Infrared Spectrometry. I. Methodology, Structural Investigation, and Water Uptake. *Biopolymers 62*, 40−53.
(45) Nobbmann, U., Connah, M., Fish, B., Varley, P., Gee, C., Mulot, S., Chen, J., Zhou, L., Lu, Y., and Sheng, F. (2007) Dynamic light scattering as a relative tool for assessing the molecular integrity and stability of monoclonal antibodies. *Biotechnol. Genet. Eng. Rev. 24*, 117−128.
(46) Liu, S. G., Liu, T., Li, N., Geng, S., Lei, J. L., Li, N. B., and Luo, H. Q. (2017) Polyethylenimine-Derived Fluorescent Nonconjugated Polymer Dots with Reversible Dual-Signal pH Response and Logic Gate Operation. *J. Phys. Chem. C 121*, 6874−6883.
(47) Kvasnov, B. A., Shalaev, P. V., and Dolgushin, S. A. (2018) in *2018 IEEE Conference of Russian Young Researchers in Electrical and Electronic Engineering (EIConRus)*, pp 1907−1909.
(48) Wu, L., Zhang, J., and Watanabe, W. (2011) Physical and chemical stability of drug nanoparticles. *Adv. Drug Delivery Rev. 63*, 456−469.
(49) Mensink, M. A., Frijlink, H. W., van der Voort Maarschalk, K., and Hinrichs, W. L. (2017) How sugars protect proteins in the solid state and during drying (review): mechanisms of stabilization in relation to stress conditions. *Eur. J. Pharm. Biopharm. 114*, 288−295.
(50) Frokjaer, S., and Otzen, D. E. (2005) Protein drug stability: a formulation challenge. *Nat. Rev. Drug Discovery 4*, 298.
(51) Mörsky, P. (1983) Turbidimetric determination of lysozyme with Micrococcus lysodeikticus cells: reexamination of reaction conditions. *Anal. Biochem. 128*, 77−85.
(52) Barbusiniski, K. (2009) Fenton chemistry - the controversies. *Ecol. Chem. Eng. S 16*, 347−358.
(53) Song, Y., Zhu, S., Xiang, S., Zhao, X., Zhang, J., Zhang, H., Fu, Y., and Yang, B. (2014) Investigation into the fluorescence quenching behaviors and applications of carbon dots. *Nanoscale 6*, 4676−82.
(54) Moyer, J., Wilson, D., Finkelshtein, I., Wong, B., and Potts, R. (2012) Correlation Between Sweat Glucose and Blood Glucose in Subjects with Diabetes. *Diabetes Technol. Ther. 14*, 398−402.
(55) Witkowska Nery, E., Kundys, M., Jeleń, P. S., and Jönsson-Niedziółka, M. (2016) Electrochemical Glucose Sensing: Is There Still Room for Improvement? *Anal. Chem. 88*, 11271−11282.
(56) Kulthong, K., Srisung, S., Boonpavanitchakul, K., Kangwansupamonkon, W., and Maniratanachote, R. (2010) Determination of silver nanoparticle release from antibacterial fabrics into artificial sweat. *Part. Fibre Toxicol. 7*, 8.

https://dx.doi.org/10.1021/acs.bioconjchem.9b00856
Bioconjugate Chem. XXXX, XXX, XXX−XXX